Mechanics & Industry **18**, 207 (2017)

DOI: 10.1051/meca/2016052
www.mechanics-industry.org

Mechanics & Industry

Tribological behavior of 304 L stainless steel used for olive oil extraction

Fatma Ben Saada[a] and Khaled Elleuch

Laboratoire de Génie des Matériaux et Environnement, LGME, Engineering school of Sfax, ENIS, University of Sfax B.P. 1173, 3038 Sfax, Tunisia

Received 2 March 2016, Accepted 14 September 2016

Abstract – Failure of equipment for processing olives interrupted oil production after only three weeks due to tribocorrosive wear of stainless steel components. Tribological behavior of 304 L stainless steel sliding against 52 100 steel was determined using a pin on disc tester. Tribological tests have shown that both normal load and rotating speed have a distinct effect on friction and wear behavior of the studied steel. An abrasive wear mechanism and plastic deformation of stainless steel on the wear track were investigated via an optical microscopy analysis. The concept of dissipated energy showed a significant correlation between the mass loss and the dissipated energy during the contact of the friction test. Then tribological behavior of 304 L stainless steel sliding against olive wood was studied. The steel was sensitive to tribo-oxidation, mostly due to abrasion by wood which presents a similar material to olive seed.

Key words: 304 L / wear / tribo-oxidation / friction / abrasion / plastic deformation

1 Introduction

Wear is regarded as a critical factor influencing the service life and even the performance for food processing, orthopedic implants, nuclear fuel reprocessing and many other industrial applications [1–3]. It is reflected by a loss of surface material due to mechanical interaction between two or more bodies in sliding contact [4, 5]. Designers and engineers always make optimal decisions to enhance material durability and solve industrial wear problem. Despite many interesting solutions, particularly in the area of olive oil industry, degradation phenomenon of material surfaces still exists. One of the steps in the olive oil extraction process is the olive crushing to obtain a paste composed by a solid part (olive seeds and vegetable rests) and other liquids (oil and water) by means of hammer crusher (Fig. 1).

Olives are introduced into the crusher chamber which received an inflow of about 30 kg.h^{-1} from a hopper. The eight hammers are positioned onto the shaft of the motor which is fixed inside the chamber. The hammers crush the olives against a counter beater (height = 5 mm) and a stationary grid with holes (Ø = 5 mm). The rotating speed of the hammers is 3000 rpm according to the designer of the machine. The centrifugal force applied by the seed on the hammer is about 44 N.

[a] Corresponding author:
fatma.ben.saada@hotmail.com

This process results in a serious problem of the total damage of the hammers, which occurs after three weeks of operation in average under severe mechanical action. Three weeks operation corresponds to 21.6×10^6 cycles with a mean time production of 8 h per day. Figure 2 shows optical observations of worn hammer.

A critical change of geometry is noticed. Such changes are referred to wear and deformation. Wear is due to the removal of metal amounts by abrasions. Seed particles, interposed between the hammer and the counter beater, are the main responsible of abrasive wear phenomenon, while plastic deformation occurs when high pressures are exerted by the hammer to cut olive due to the high rotating speed [6]. Some points of oxidative wear are shown in the surface of worn hammer.

Various steel grades were tested for a more resistant material and the 304 L stainless steel was recently performed by the industry. However, the wear problem of hammers still persisted. Consequently, it is necessary to replicate this damage in laboratory scale by testing material with pin on disc tribometer. The rotating hummer can be simulated with a rotating disc fixed in engine axe of tribometer as well as the pin takes the role of seed particle.

In literature [7–20] normal load and sliding speed were the appropriate parameters in friction and wear studies. Therefore, an attempt is made to investigate these parameters effect on wear behavior of 52 100 steel against

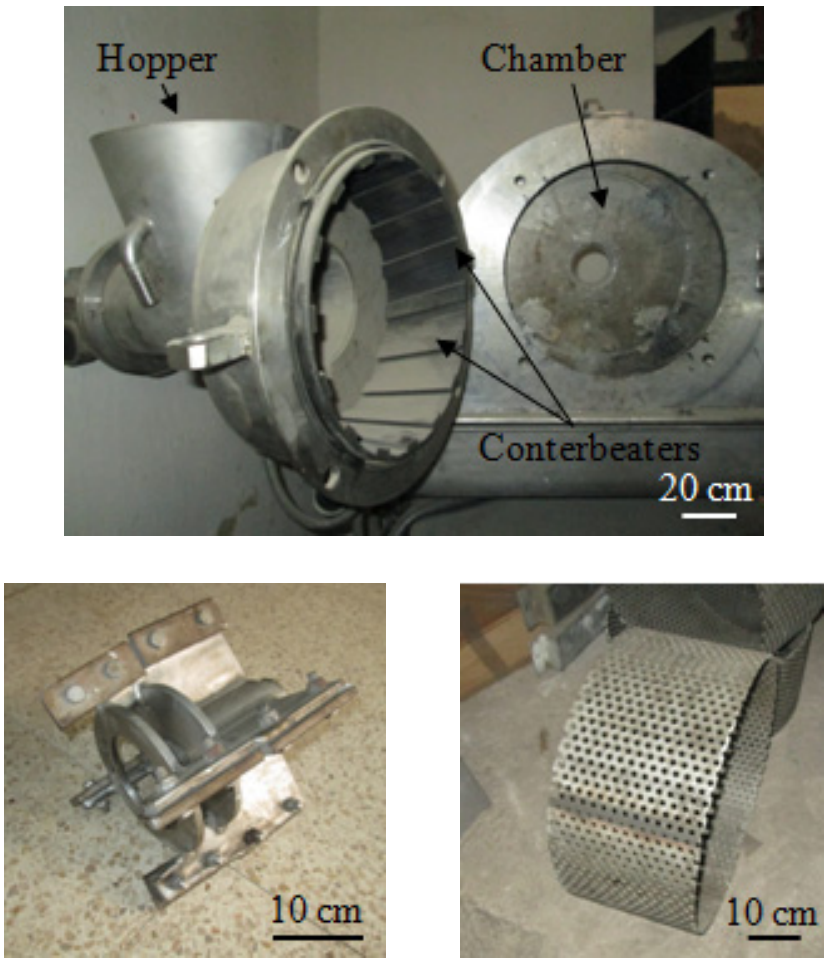

Fig. 1. Hammer crusher: (a) Chamber (b) Hammers and (c) Grid.

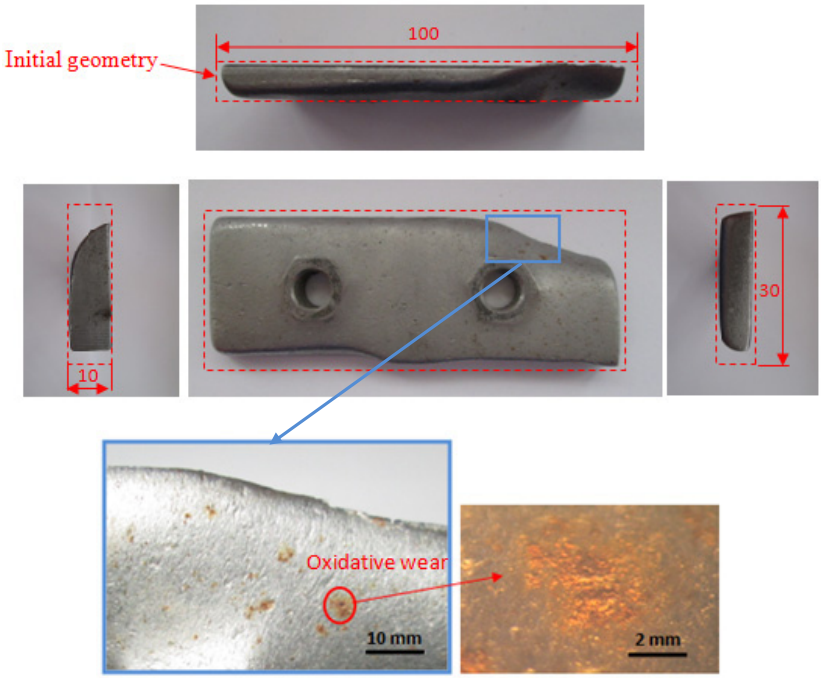

Fig. 2. Worn hammer.

Fig. 3. Optical morphology of 304 L stainless steel.

stainless steel in order to reproduce the hammer wear. The objectives of this present paper is (i) to study the effect of load and speed on the reproducibility of ball on disc test results, (ii) to quantify friction and wear of stainless steel under rotating sliding and (iii) to determine a possible relationship between wear volume and dissipated energy under friction.

2 Materials and methods

2.1 Specimens and surface preparation

Experiments were performed on 304 L stainless steel. It is an austenitic stainless steel with face-centered cubic crystallographic structure. It is characterized by a Young's modulus of about 200 GPa and microhardness of about 170 ± 7 HV with a load of 10 N and a dwell time of 15 s.

The material is provided in form of plates with a thickness of 9 mm. Specimens were cut in a square shape of 20 mm in length per side for tribological tests. They were mechanically polished with SiC papers up to 1200 grade to have a roughness of R_a = 011. Then, they were ultrasonically cleaned in distilled water, degreased with acetone and dried to be prepared for the tribological tests.

Morphology observation was carried out on surface material before test and the cross section of wear track. The surface was polished with several grades of alumina pastes grade down to 1 μm to obtain a mirror surface (Ra = 0.08 μm). The optical micrographs in Figure 3 show a microstructure with a mean grain size of approximately 20 μm. Such a structure was also observed by Goutie et al. [21].

2.2 Tribological measurement

The wear tests were performed on a pin on disc tribometer. It consists mainly of a 52 100 steel ball with a diameter of 6 mm and a surface roughness of Ra = 0.03 μm fitted on the top of a horizontally rotating disc. The cleaning process of the 52 100 steel balls is similar to specimens one. The stationary ball was loaded under a dead weight. The disc was driven by a d. c. motor. The tangential force originating from the normal force was measured on-line by a load sensor (strain gauge). The load sensor ranges from 0.5 to 10 N. The test was repeated three times and friction coefficient μ was represented versus time. The testing conditions used in this study are listed in Table 1.

The normal force was applied by a dead weight. The maximum compressive contact pressure was calculated using the following expression [22].

$$\sigma_{\max} = \left[\frac{6\,P\,(E^*)^2}{\pi^3\,R^2}\right]^{\frac{1}{3}} \tag{1}$$

where

$$\frac{1}{E^*} = \frac{1-\gamma_1^2}{E_1} + \frac{1-\gamma_2^2}{E_2} \tag{2}$$

with P the applied load, R the radius of the ball, $E_{1,2}$ the young's modulus 200 and 210 (GPa) and $\gamma_{1,2}$ Poisson's ratio 0.27 and 0.3 of specimen 304 L stainless steel and ball 52 100 steel, respectively. Hertzian contact pressure and area for a point contact (σ_x) at the different normal loads are presented in Table 1. These pressures confirmed that the considered contact is plastic ($\sigma_x > 1.1\sigma_y$) where σ_y = 209 MPa. The 304 L stainless steel is deformed plastically at the static contact area by applying these normal loads. The real contact area of seed particles depends on its sizes which are between 1 and 6 mm of diameter. Their contact pressures range between 1528 and 5046 MPa. This real pressure is higher than the maximum pin pressure at static contact. Thus, the tribological answer of the surfaces with the variation of friction is only studied by varying rotating speed from 0.052 to 0.209 (m.s^{-1}).

After the friction test, wear debris were recovered with a transparent adhesive tape. Typical optical micrographs of wear track were performed for wear track and its cross-section. The wear track parameters (width, depth and area) were determined from optical morphology of the cross section. Then specimens were cleaned ultrasonically in ethanol to remove the loose wear debris for quantitative analyses. Quantitative wear was performed using mass loss measurements on a balance with a 0.01 mg precision.

3 Results et discussions

3.1 Influence of the normal load on tribological behavior and wear

In this section, the variation of normal load is carried out in the range of 1 to 8 N using a speed of 0.052 m.s^{-1}. Figure 4 shows a superposition of friction coefficient curves for all tests. The highest steady state of friction coefficient 1.15 is observed at a normal load of 1 N. This steady state decreases with normal load to reach 0.65 at 8 N.

Table 1. Summary of the test conditions.

Normal load (N)	1, 2, 4, 8
Maximum Hertzian contact pressure (MPa)	644, 811, 1022, 1290
Hertzian contact area (10^3 mm^2)	2.3, 3.7, 5.9, 9.3
Wear track diameter (m)	0.01
Speed (rpm)	100, 200, 300, 400
(m.s^{-1})	0.052, 0.104, 0.157, 0.209
1 cycle (s)	0.6, 0.3, 0.2, 0.15
Testing environment	Ambient air
Temperature (°C)	24
Relative Humidity HR (%)	35

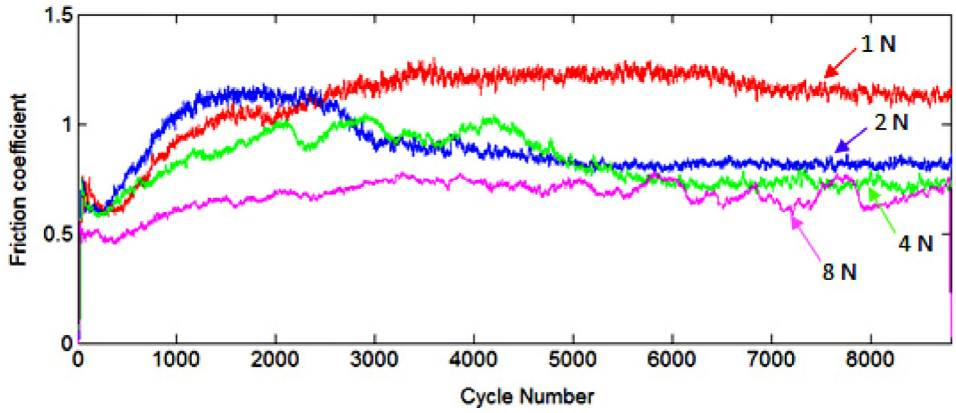

Fig. 4. Friction coefficient as a function of cycle number at different normal loads, rotating speed (rpm): 0.052 m.s^{-1}, HR (%: 35).

Typical data on the variation of friction vs. cycle number of the 304 L stainless steel/52100 steel contact are shown in Figure 5a under a normal load of 1 N. After friction test, the wear debris were recovered with a transparent adhesive tape (Fig. 5b). Figure 5a shows that the friction coefficient undergoes three phases at a rotating speed of 0.052 m.s^{-1}: contact establishment (Ph.1), friction coefficient increase (Ph.2) and friction coefficient stabilization (Ph.3). The contact establishment corresponds to the maximum surface between specimen and ball. The time from start to the transition point is specifically defined as a gestation period [24]. Visual observation during gestation period showed that the wear track appeared with dark grey debris at cycle number 330. Such phenomenon was accelerated with the increase of the normal load. It became 166 cycles for 8 N. After contact establishment, the friction coefficient rose to a steady state. The continuous filming of the wear track showed that the dark grey debris were expected from the contact at 1666 cycles. Then the color of wear track and debris was changed to brown at 2000 cycles. These phenomena were accelerated with normal load. At 8 N, debris were expelled from the contact at 666 cycles and brown color wear track and debris appeared at 1166 cycles. After that, friction coefficient stabilized at 1.2, at a normal load of 1 N. During phase (Ph.3), the color of the wear track and debris was still brown which indicate a surface oxidation phenomenon. In fact, the oxide layer is continuously rubbed away from the subsurface material. The metallic surface is always exposed to the oxidation process promoted by ambient conditions [25–28].

Huq and Celis applied a wide range of normal load and revealed a change in the friction coefficient with varying loads [22]. In agreement with Huq and Celis, Bowden and Tabor also reported a declining friction coefficient with an increasing load when testing indium films on steel and extended their interpretation to explain experiments with oxide-covered surfaces [29]. Their explanation was that the friction force is not linearly proportional to the normal load. Other possible causes might be that the increasing load produces an increasing wear, which in turn causes a surface roughening or generates a wear debris layer which modifies the shear-strength of the interface between the two first contacted bodies [22].

Figure 6 shows wear tracks for specimens tested at 1 and 8 N for a rotating speed of 0.052 m.s^{-1}. Shallow scratches and grooves on the worn surfaces, parallel to sliding direction, indicate abrasive wear mechanisms At the beginning, the scenario of wear mechanism was conducted by two-body abrasion due to the sliding of 52 100 steel ball (300 HV) against a softer 304 L stainless steel (170 HV). Then grey debris were created from destroyed passive film. When the passive film was completely removed oxide debris were generated from base material. Moreover, material transfer proves an adhesive wear mechanism (Fig. 6b). Adhesion occurred between asperities at contact interface due to the friction force caused by the sliding interaction. Asperities of soft

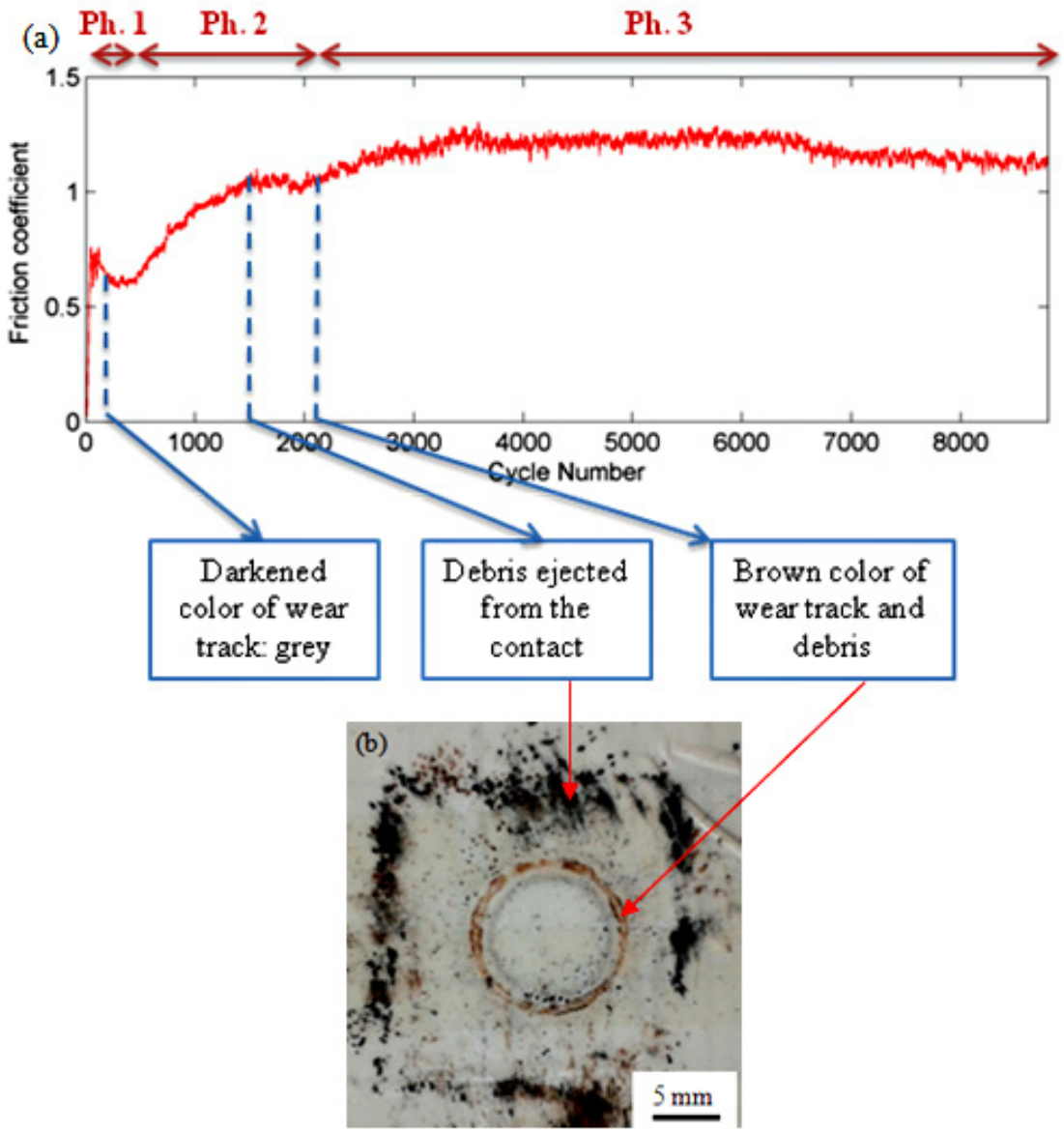

Fig. 5. (a) Friction coefficient as a function of cycle number and (b) description of wear products at 1 N and 0.052 m.s^{-1}, HR (%): 35.

material were plastically deformed and transferred to the harder material. In addition to local adhesion, the profile section of wear track was characterized by plastic deformation under the effect of ball penetration (Fig. 7). The deformation increases with normal load by the presence of wedges especially at 8 N as shown in Figure 7b.

Consequently, plastic deformation, abrasive and adhesive mechanisms were more pronounced at high normal load. A higher load created deeper plough abrasive marks and more adhesive bonds although the low friction coefficient (Fig. 5). This could be explained by the effect of oxide debris. Under high pressure, the oxide debris probably stay in contact to act as a solid lubricant.

At this point, a quantification of the observed wear was performed. Figure 8 shows mass loss versus normal load at 0.052 m.s^{-1}. An increase of mass loss is noticed with increasing normal load. The applied load value plays a significant role in the amount of material loss [30]. The amount of particles as a third body coming from the specimen surface increases with the higher normal load. These particles remain between the specimen surface and the counter body. Thus, plenty particles result in an extensive wear for higher load levels. At lower load level, the particles scrape the specimen surface less than at higher load levels.

The increase of wear rate with normal load at 0.052 m.s^{-1} is explained by the increase of the width L_w, depth Z_w and area S_w of the wear track (Tab. 2). The possible reason for increasing mass loss with normal load is that during tests, the contact area between bodies increased due to friction wear which caused an increase of the interaction between contacting materials [22, 23].

Table 2. Width L_w, depth Z_w and area S_w of track wear at different conditions.

Rotating speed (m.s^{-1})	Normal load (N)	L_w (μm)	Z_w (μm)	S_w (μm^2)
0.052	1	170 ± 41	4 ± 2	536 ± 52
	2	214 ± 20	3 ± 3	765 ± 31
	4	428 ± 15	8 ± 3	2062 ± 45
	8	433 ± 37	12 ± 9	3046 ± 120

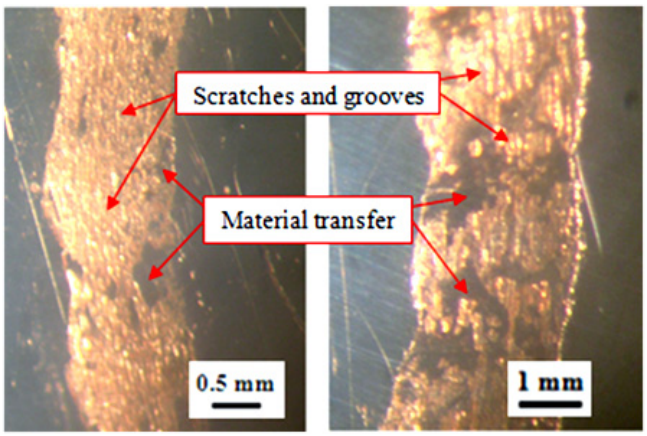

Fig. 6. Wear track at 0.052 m.s^{-1} and different load conditions. (a) At 1 N and 0.052 m.s^{-1} and (b) At 8 N and 0.052 m.s^{-1}.

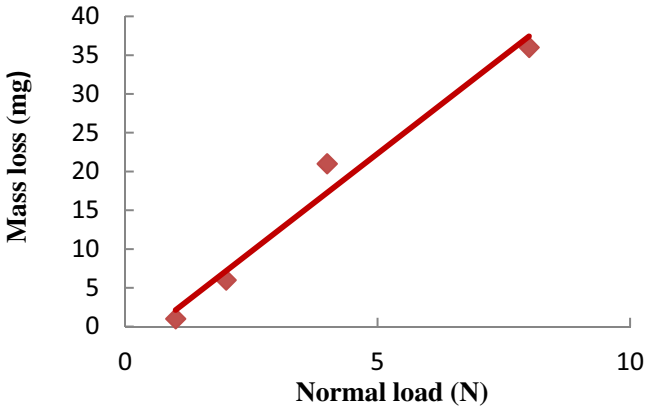

Fig. 8. Mass loss measurements as a function of normal load for 304 L stainless steel sliding against 52100 steel ball (0.052 m.s^{-1}).

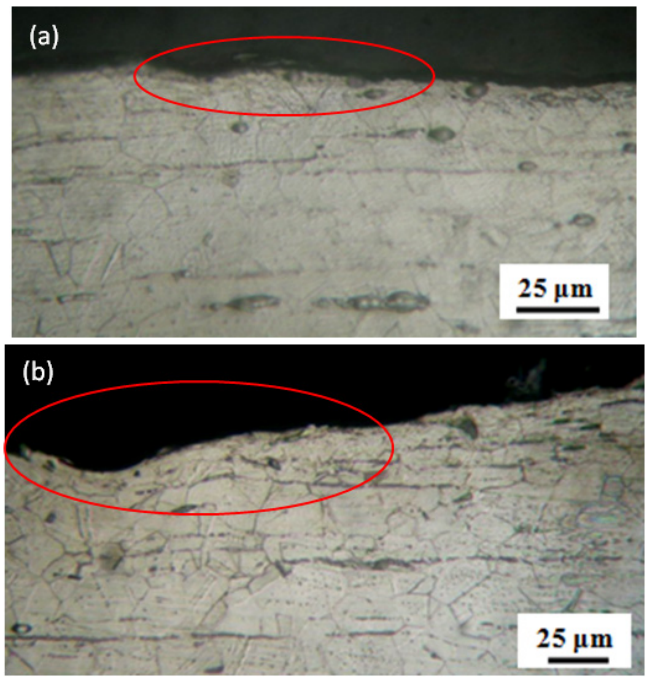

Fig. 7. Morphology observation of cross-section of the wear tracks at 0.052 m.s^{-1} (a) at 1 N and (b) at 8 N.

3.2 Influence of the rotating speed on tribological behavior and wear

In this section the variation of the rotation speed is carried out in the range of 0.052 up to 0.157 m.s^{-1} using a normal load of 2 N. Figure 9 shows that the friction coefficient undergoes three phases at lowest rotation speed (0.052 m.s^{-1}): contact establishment (Ph.1), increase of friction coefficient (Ph.2) and μ stabilization (Ph.3).

At a high rotation speed (0.104 and 0.157 m.s^{-1}), the second phase is not clear in the friction curves because the increase of the friction coefficient was accelerated and a passive film was rapidly eliminated. In addition, the highest rotation speed inhibits the interaction of worn surface with environment. In fact there is no variation of the friction coefficient after the contact establishment. Typical data on the friction variation versus the cycle number of 304 L stainless steel/52 100 steel contacts under a rotation speed of 0.104 m.s^{-1} are shown in Figure 10.

Figure 10a shows that the friction coefficient undergoes only two phases: establishment of contact and stabilization of μ. Macroscopic observations of wear debris show that wear track with dark grey color is observed at 6250 cycles. After 250 cycles, the debris are created and ejected from the contact. At 6750 cycles, they comprise both metallic grey particles and brown oxides as shown in Figure 10b. That observation was accelerated with the rotating speed decrease. For instance, at 0.052 m.s^{-1}, such phenomenon occurred at 2500 cycles. Moreover, at higher rotation speed (typically 0.157 m.s^{-1}) the debris are completely metallic in nature with a bright grey color. As the rotation speed decreases, more time is allowed for the interaction of the wear track with environment in ambient conditions [24] and oxides layers are then formed [25].

Using the experimental findings of the present investigation together with the information from the literature [23, 24], the wear evolution of the materials under friction seems to follow three stages. The first stage

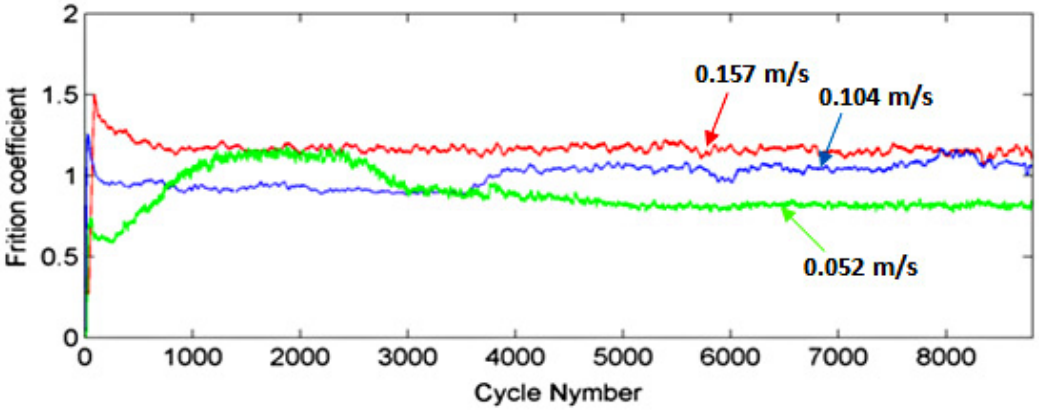

Fig. 9. Friction coefficient as a function of time at different rotating speeds, normal load (N): 2, HR (%): 35.

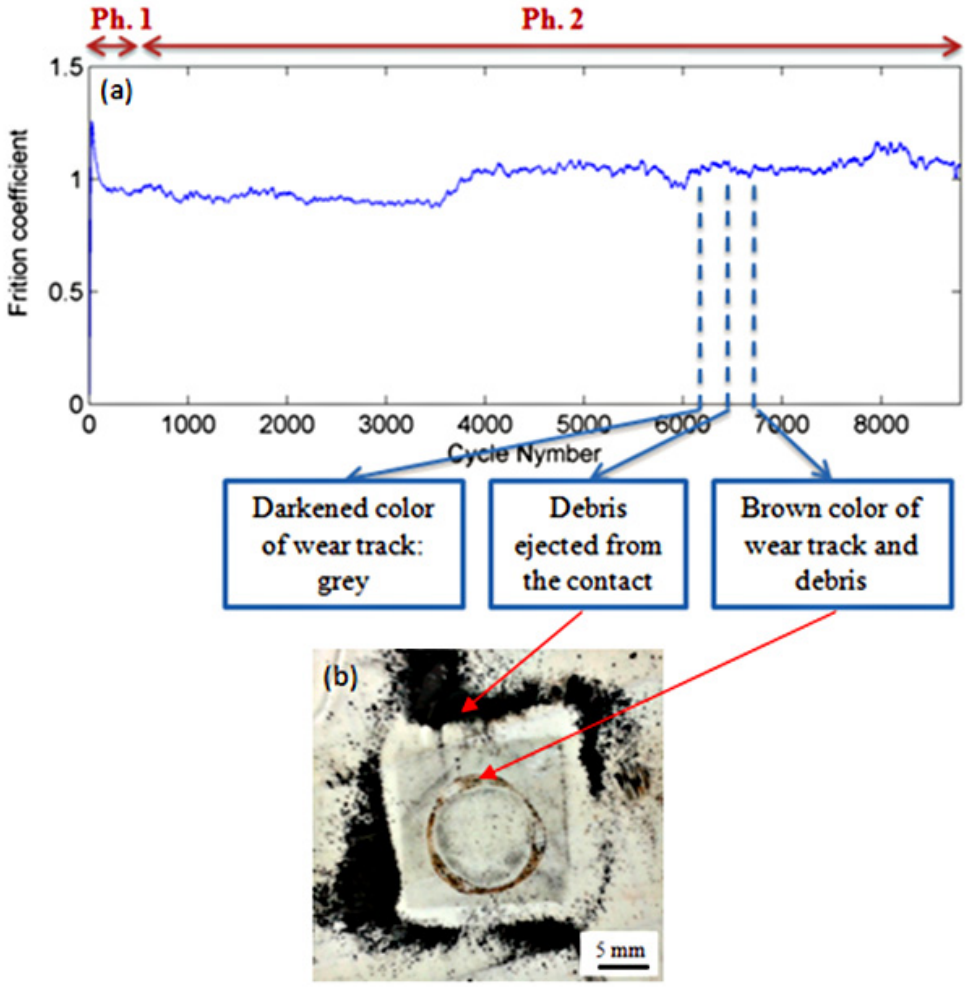

Fig. 10. (a) Friction coefficient as a function of cycle number and (b) description of wear products at 2 N and 0.104 m.s^{-1}, HR (%): 35.

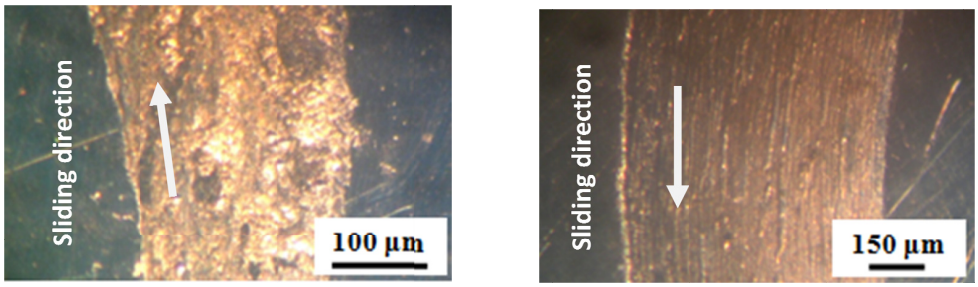

(a) (b)

Fig. 11. Wear track at 2 N and different rotating speeds. (a) At 2 N and 0.052 m.s^{-1} and (b) At 2 N and 0.104 m.s^{-1}.

corresponds to the formation of tribological layers. The formation of such layers is attributed to the plastic deformation of the contact surface induced by friction forces reaching a critical plastic strain at the external part of the subsurface plastic sheared region. In fact, optical observation carried out at 0.052 m.s^{-1} revealed an accumulation of transferred material on surface as shown in Figure 11a. Morphology observation of the wear track cross-section confirmed that friction induced a plastic deformation on the surface layer and especially passive film (Fig. 12a). This deformation increases with rotating speed by the presence of wedges and Tribologically Transformed Surfaces (TTS).

Figure 12b shows three areas which are a superficial area formed by oxide debris trapped in the contact, the TTS area and a plastically deformed area. The intensity and depth of the plastic deformation increased with rotating speed from about 5 μm at 0.052 m.s^{-1} to 15 μm at 0.104 m.s^{-1} (Fig. 12b). Consequently, debris during friction were detached from the tribological layer with 5 μm thickness at 0.104 m.s^{-1}.

The second stage is the formation of wear debris by abrasion. Abrasive sliding marks, scratches and grooves on the wear tracks in the direction of friction prove that the wear mechanism is abrasion (Fig. 11). Consequently, the amount of debris which was continuously created increased with rotating speed. This fact explains the absence of transferred material in the wear track which is eliminated continuously by abrasion at higher rotating speed (Fig. 11b). The third stage consists of the oxidation of the produced wear. In fact the oxidized debris are trapped in the contact between the specimen and the ball. They form a layer that varies in its thickness with the gathering of very fine particles, thus causing wear by tribo-oxidation.

The wear quantification of the 304 L stainless steel rubbing against 52 100 steel was studied. The mass loss versus the rotation speed at 2 N is shown in Figure 13. The mass loss increased with the rotating speed. The increase of rotating speed caused a rise in the amount of wear debris. This is due to the increase of width L_w depth Z_w and area S_w of the wear track with the rotation speed already noticed with the optical observation (Tab. 3).

3.3 Wear

From the above experimental study it can be deduced that abrasion is the main wear mechanism for all the studied conditions. It was accompanied with adhesive wear by the subsurface plastic deformation, the presence of wedges and the material transfer. The origin of this wear phenomenon is often explained by the accumulation of dissipated energy induced by a plastic deformation in the subsurface layer which gives rise to a tribological transformed surface [31,32]. When comparing the wear values measured at different test conditions no obvious relationship between normal load and sliding speed was found. In fact, the wear rate increases with normal force for the tests carried out at 0.052 m.s^{-1}. However, at 0.157 m.s^{-1} the variation of the normal load doesn't cause the expected evolution of the wear rate. On the other hand, it was found that the friction coefficient increases with rotation speed under a low normal load. However it decreases with the rotation speed under high normal load. Such results could be explained by the formation of an adhesion junction on the interface (ball/specimen). In fact, at high normal load, a hard junction is formed. In contrast, at low normal load weak junctions are formed. A soft junction is noticed as well when the rotation speed increases. Indeed as the rotation speed increases, the shear stress required to separate the junction decreases [24].

A synthetic representation of the wear rate of 304 L stainless steel rubbed against 52 100 steel as function of both normal load and rotation speed is shown in Figure 14.

No evident correlation between wear and the variation of the normal load and the rotation speed is noticed. Normal load rise induces monotonic wear increase for each rotating speed. However, wear has different evolution as a function of rotating speed under constant load. Particularly at 4 N wear decreases with rotating.

Recent studies have shown that energy approach displays a higher stability when describing the wear rate versus both normal load and sliding speed [31–33]. The energy dissipated in the contact can be calculated as the work of the friction force. For each time interval Δt, which corresponds to a displacement Δx, the dissipated energy ΔE can be found with Equation (3). Considering the mean value of the friction force and assuming a constant

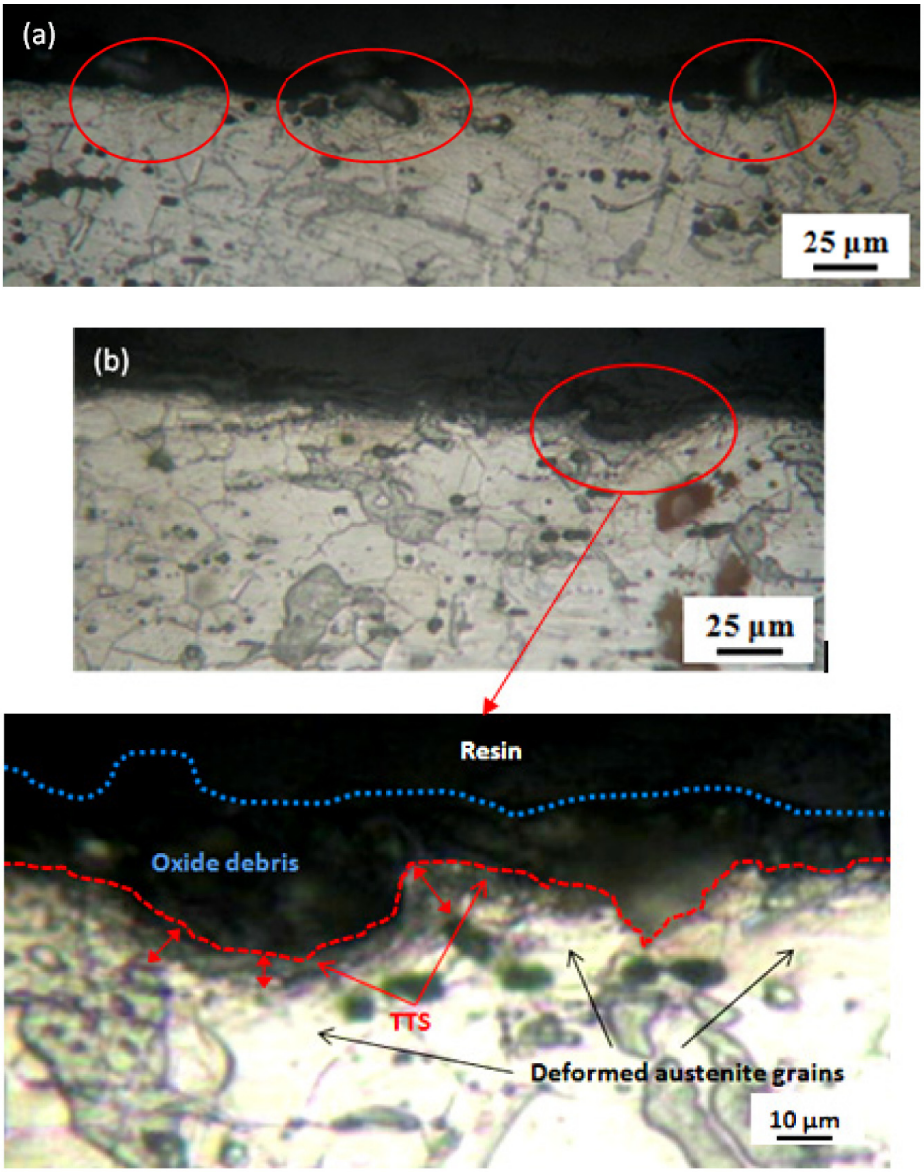

Fig. 12. Morphology observation of cross-section of the wear tracks at 2 N for rotating speed: (a) 0.052 and (b) 0.104 m.s^{-1}.

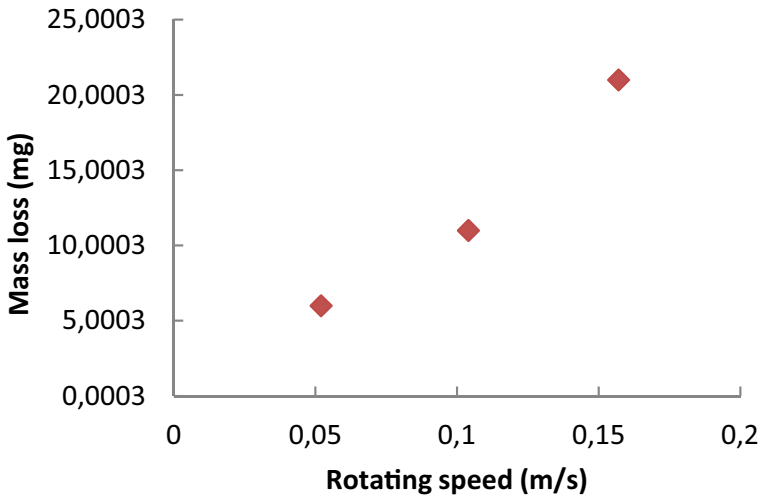

Fig. 13. Mass loss measurements as a function of rotating speed for 304 L stainless steel sliding against 52100 steel ball (2N).

Table 3. Width L_w, depth Z_w at area S_w of track wear at different conditions.

Normal load (N)	Rotating speed (m.s^{-1})	L_w (μ m)	Z_w (μ m)	S_w (μ m^2)
2	0.052	214 ± 30	3 ± 6	765 ± 80
	0.104	404 ± 15	16 ± 3	3402 ± 31
	0.157	580 ± 64	20 ± 5	7750 ± 95

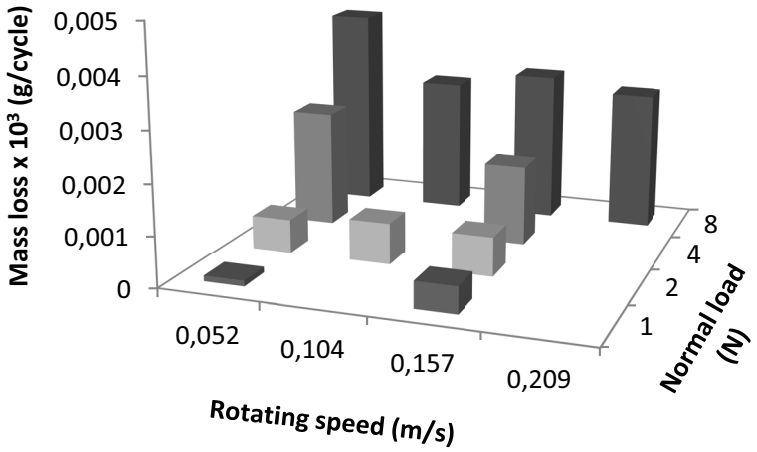

Fig. 14. Wear mass on 304 L stainless steel after rotating tests against 52 00 steel ball performed at room temperature and at various conditions.

sliding speed, Equation (4) can be used [34]:

$$\Delta E = \int_0^{\Delta t} F\,\mathrm{d}x = \int_0^{\Delta t} F\,V\,\mathrm{d}t \tag{3}$$

$$\Delta E = \bar{F}\,V\,\Delta t \tag{4}$$

with $\bar{F}$ the average value of the friction force and V the sliding speed.

The cumulative friction energy Ed, Equation (5) can be calculated in ball-on-disc equipment by the following relationship [28]:

$$E_d = F_t d = \mu\,F_n\,V\,t \tag{5}$$

with F_t, the tangential force, d the sliding distance, μ the friction coefficient, F_n the normal load, V the sliding speed, and t the test duration.

An energetic approach was applied to all the tested cases. A linear relationship between the dissipated energy and the cumulative wear on the 304 L was found and this relationship was not affected by different load and speed conditions as shown in Figure 15.

Yet, there is a significant correlation between the wear and the dissipated energy through interfacial friction and wear processes. The wear can be predicted from the friction coefficient and test conditions [22,35]. It still confirms the reliability of the dissipated energy density approach to predict the wear loss of the tested specimens. A linear regression leads to a β_v value equal to $\beta_v = 0.018$ g/N*m for the studied 304 L/52 100 steel contact. A pin on disc tribometer can be used with normal load of 4 N and rotating speed of 0.052 or 0.104 m.s^{-1} to replicate the centrifuge damage in laboratory scale which is characterized by tribo-oxidation, abrasive wear, and plastic deformation.

3.4 Tribological Behavior of wood on 304 L stainless steel

The real working conditions for oil extraction equipment are not simulated by tribological tests. In the equipment, the surfaces are always wet and loose seeds are in contact with metal surfaces. The aggressiveness of olive juice due to acidity and salts stimulates tribo-corrosive wear. In the laboratory tests, dry sliding was realized and only oxidative wear and abrasion action of olive wood pin occurred. The choice of olive wood is based on its cellulose content. In fact, both olive wood and olive seed are rich in cellulose with a percentage of about 40% [36–38]. In addition they have a near microhardness of 14 and 8 $HV_{0.01}$, respectively. Therefore a 7 mm diameter olive wood pin with a 100 mm radius spherical tip was selected as a counterbody. The effect of olive wood on 304 L stainless steel was studied as a contact pin-on-disc tester with normal load of 4 N and rotating speed of 0.104 m.s^{-1}. Typical data for the variation of friction vs. cycle number of the AISI 304 L / wood contact are shown in Figure 16. Figure 16 shows that the friction coefficient undergoes three phases: contact establishment (Ph.1), friction coefficient increase (Ph.2) and friction coefficient stabilization (Ph.3). During the first phase, the wear track was a clear grey color. During the second phase, the friction coefficient rose to stable state, debris were expelled

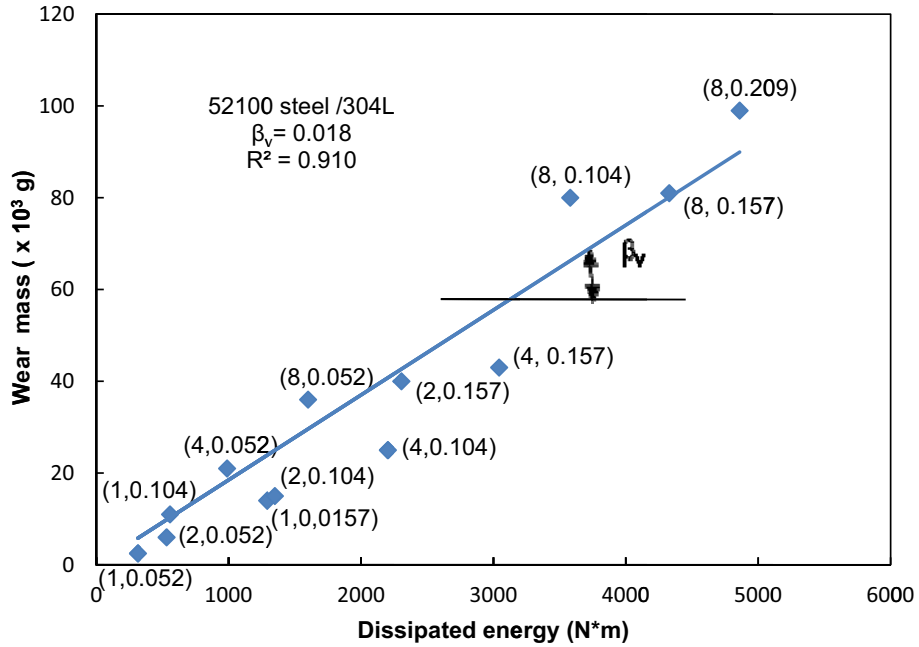

Fig. 15. Wear mass as a function of the cumulative dissipated energy on 304 L stainless steel disc tested against 52 100 steel ball at different conditions (load (N) and speed (m.s^{-1})).

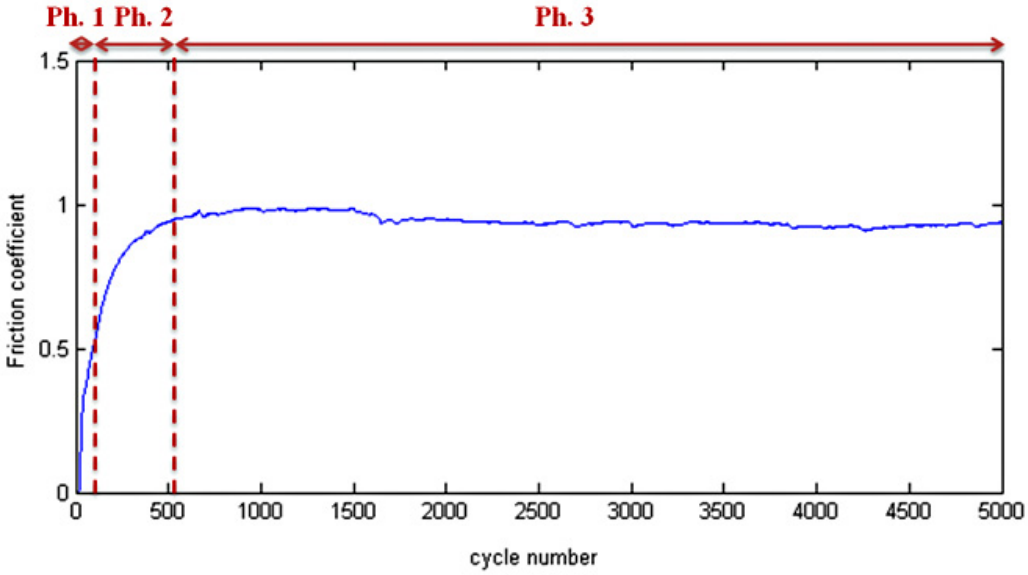

Fig. 16. Friction coefficient as a function of cycle number of AISI 304 L/ wood contact at 5 N and 100 rpm.

from the contact and the wear color changed to dark grey. During the third phase, the friction coefficient stabilized at 0.9, and the color of the wear track and debris changed to brown. This color is related to surface oxidation and indicates a tribocorrosion phenomenon such as tribo-oxidation.

After tribological tests, the total wear loss was determined and the obtained value is approximately 10.35 × 10^{-8} g.cm^{-3}. The wear track was qualitatively studied. From Figure 17a optical image shows that the wear track width is uniform. 3D profilometry image shows scratches and some plastic deformation in the surface of the wear track by the presence of wedges. These observations are confirmed in scanning electron microscope image by the presence of shallow scratches and some grooves parallel to the sliding direction as shown in Figure 18. Although the wood seed microhardness is very small compared to that of 304 L stainless steel, it seems that the olive woods and, eventually, wear particles removed material by an abrasive wear mechanism. Moreover, the effect of mechanical

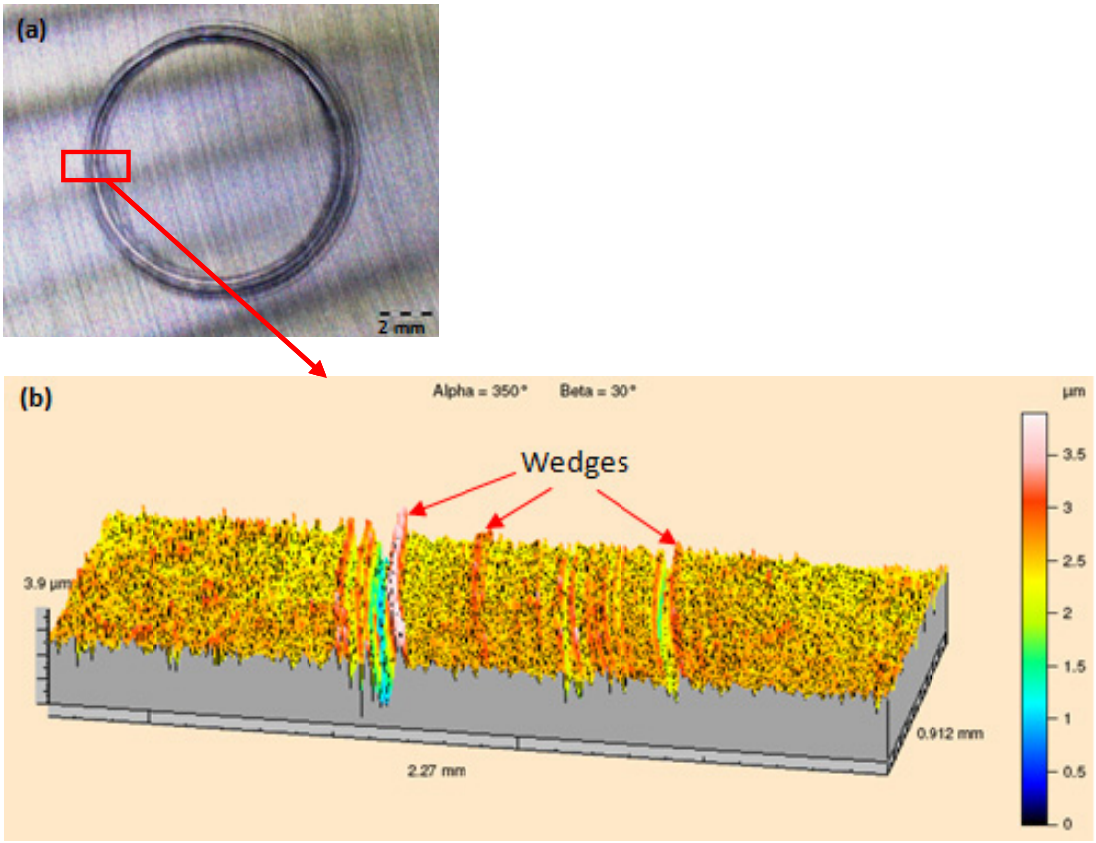

Fig. 17. (a) Optical micrograph and (b) 3D profilometry dimensional image of the wear track after 304 L/wood friction.

action is detected by the microhardness in the wear track. Microhardness was greater on worn surfaces than unworn surfaces. In fact, microhardness was about 312 $HV_{0.05}$ and 280 $HV_{0.05}$ on worn and unworn surface, respectively. The surface layer of the steel was work hardened.

The tribological test suggests that the major factor is the mechanical action of olive wood. The most probable reason is the abrasive wear by a three body mechanism caused by wood and wear products that work-hardened surfaces in contacts.

4 Conclusions

Severe wear of olive processing equipment leads to severe failure after a short operating time due mostly to mechanical damage by the impact of olive seed particles. The tribological behavior of the 304 L stainless steel rubbed against the 52 100 steel was investigated in this study. It was found that there is no obvious relationship between the friction coefficient and test parameters (normal load, rotation speed). The main wear mechanism of the 304 L stainless steel exhibited an abrasive wear accompanied by a plastic deformation, the formation of beads and a tribological transfer layer. Hence an energy approach was considered. A significant correlation was found between the wear rate and the dissipated energy in the contact A pin on disc tribometer can be used with normal load of

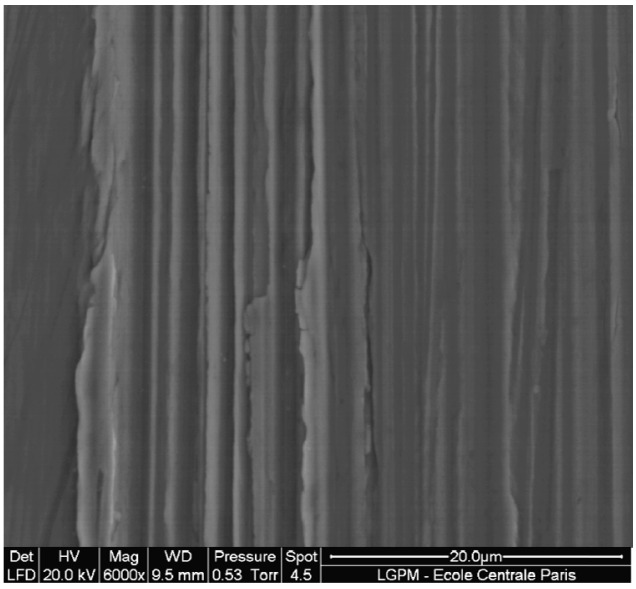

Fig. 18. Scanning electron microscope observations of the wear track after 304 L/wood friction.

4 N and rotating speed of 0.104 $m.s^{-1}$ to replicate the centrifuge damage in laboratory scale. Moreover, the effect of olive wood on stainless steel was determined because wood is a cellulosic material such as olive seed. Olive wood

caused tribo-oxidation, abrasive wear, and plastic deformation. Olive wood counterbody combined with severe operating conditions may lead to material failure caused by abrasive wear and surface degradation

Acknowledgements. This work was partially supported by EU-FP7 grant Oil&Sugar (295202). Also, the present authors thank LGPM – Ecole Centrale Paris for surface analyses.

References

[1] Y.Y. Özbek, M.Durman, H. Akbulut, Wear Behavior of AISI 8620 Steel Modified by a Pulse-Plasma Technique, Tribol. Trans. 52 (2009) 213–222

[2] J.R. Laguna-Camacho, L.Y. Villagran-Villegas, H. Martınez-Garcia, G. Juarez-Morales, M.I. Cruz-Orduna, M. Vite-Torres, L. Rios-Velasco, I. Hernandez-Romero, A study of the wear damage on gas turbine blades Engineering Failure Analysis, 2015

[3] S.M. Zamani, S.A. Hassanzadeh-Tabrizi, H. Sharif, Failure analysis of drill pipe: A review, Eng. Failure Anal. 59 (2016) 605–623

[4] M. Ibrahim, M. Deiaba, A. Elbestawi, Experimental determination of the friction coefficient on the workpiece-fixture contact surface in workholding applications, Int. J. Machine Tools Manuf. 45 (2005) 705–712

[5] M.Z. Huq, J.-P. Celis, Expressing wear rate in sliding contacts based on dissipated energy, Wear 252 (2002) 375–383

[6] F.B. Saada, K. Elleuch, Damage of stainless steel components by olive paste, Tribol. Trans., DOI: 10.1080/10402004.2015.1115569

[7] P.L. Menezesa, Kishorea, S.V. Kailasb, Influence of surface texture and roughness parameters on friction and transfer layer formation during sliding of aluminum pin on steel plate, Wear 267 (2009) 1534–1549

[8] S.V. Kailas, P.L. Menezes, Coefficient of friction and material transfer studies of an Al–Mg alloy pin on EN8 steel flat using inclined scratch, Proceedings of International Seminar on Metal Forming-Process Design and Optimization (2003) 124–143

[9] D.K. Dwivedi, T.S. Arjun, P. Thakur, H. Vaidya, K. Singh, Sliding wear and friction behavior of Al–18% Si–0.5% Mg alloy, J. Mater. Process. Technol. 152 (2004) 323–328

[10] S.C. Lim, M.F. Ashby, J.H. Brunton, The effects of sliding conditions on the dry friction of metals, Acta Metall. 37 (1989) 767–772

[11] J.M. Lanzon, M.J. Cardew-Hall, P.D. Hodgson, Characterising frictional behavior in sheet metal forming, J. Mater. Process. Technol. 8081 (1998) 251–256

[12] I. Nogueira, A.M. Dias, R. Gras, R. Progri, An experimental model for mixed friction during running-in, Wear 253 (2002) 541–549

[13] T. Kayaba, A study of the wear and friction of some bearing materials, Wear 5 (1962) 173–181

[14] M.O.A. Zaki, G.S.A. Shawki, Effect of mechanical properties on frictional behaviour of metals, Tribol. Int. 12 (1979) 265–268

[15] Z. Rymuza, Energy concept of the coefficient of friction, Wear 199 (1996) 187–196

[16] P.L. Menezes Kishore, S.V. Kailas, Effect of surface topography on friction and transfer layer during sliding, Tribol. Online 3 (2008) 25–30

[17] M.R. Lovell, Z. Deng, M.M. Khonsari, Experimental characterization of sliding friction: crossing from deformation to plowing contact, Trans. ASME 122 (2000) 856–863

[18] D.H.H. Wang, K.H.Z. Gahr, Transition from static to kinetic friction of unlubricated or oil lubricated steel/steel, steel/ceramic and ceramic/ceramic pairs, Wear 255 (2003) 365–375

[19] H.D. Fridman, P. Levesque, Reduction of static friction by sonic vibrations, J. Appl. Phys. 30 (1959)1572–1575

[20] K. Hiratsuka, A. Enomoto, T. Sasada, Friction and wear of $A1_2O_3$, ZrO_2 and SiO_2 rubbed against pure metals, Wear 153 (1992) 361–373

[21] F. Goutier, S. Valette, A. Vardelle, P. Lefort, Oxidation of stainless steel 304 L in carbon dioxide, Corros. Sci. 52 (2010) 2403–2412

[22] K.L. Johnson, Contact Mechanics, Cambridge University Press, 1985

[23] M. Hua, X. Wei, J. Li, Friction and wear behavior of SUS 304 austenitic stainless steel against Al_2O_3 ceramic ball under relative high load, Wear 265 (2008) 799–810

[24] G. Straffelini, A. Molinari, D. Trabucco, Sliding wear of austenitic and austenitic-ferritic stainless steels, Metall. Mater. Trans. A 33 (2002) 613–624

[25] A. Van Herpen, B. Reynier, C. Phalippou, Effect of test duration on impact/sliding wear damage of 304 L stainless steel at room temperature: metallurgical and micromechanical investigations, Wear 249 (2001) 37–49

[26] T.F.J. Quinn, Review of oxidational wear, Trib. Int. 16 (1983) 306–315

[27] D. Wei, J. Huang, A. Zhang, Z. Jiang, A. Tieu, F. Wu, X. Shi, S. Jiao, Deformation of oxide scale and surface roughness transfer during hot rolling of stainless steel 304 L Science, Eng. Technol. 3 (2009) 459-470

[28] W. Hubner, A. Pyzalla, K. Assmus, E. Wild, T. Wroblewski, Phase stability of AISI 304 stainless steel during sliding wear at extremely low temperature, Wear 255 (2003) 476–480

[29] F.P. Bowden, D. Tabor, The Friction and Lubrication of Solids, Oxford Science. Oxford (1986) 119–120

[30] H. Cetinela, E. Celikb, M. Kusoglub, Tribological behavior of Cr2O3 coatings as bearing materials, J. Mater. Process. Technol. 196 (2008) 25–265

[31] M. Estevesa, A. Ramalhoa, F. Ramosb, Fretting behaviour of the AISI 304 stainless steel under different atmosphere environments, Tribol. Int. (2015)

[32] S. Fouvry, Ph. Kapsa, L. Vincent, Quantification of fretting damage, Wear 200 (1996) 186–205

[33] S. Fouvry, Ph. Kapsa, An energy description of hard coatings wear mechanisms, Surf. Coat. Technol. 138 (2001) 141–148

[34] A. Ramalhoa, J.C. Miranda, The relationship between wear and dissipated energy in sliding systems, Wear 260 (2006) 361–367

[35] N. Guermazi, K. Elleuch, H.F. Ayedi, V. Fridrici, Ph. Kapsa, Tribological behaviour of pipe coating in dry sliding contact with steel, Mater. Design 30 (2009) 3094–3104

[36] J. Fernfindez-Bolafios, B. Felizon, A. Heredia, R. Guillin, A. Jimnez, Characterization of the lignin obtained by alkaline delignification and of the cellulose residue from steam-exploded olive stones, Bio-resource Technol. 68 (1999) 121–132

[37] C. Cara, E. Ruiz, I. Ballesteros, M.J. Negro, E. Castro, Enhanced enzymatic hydrolysis of olive tree wood by steam explosion and alkaline peroxide delignification, Process Biochemistry 41 (2006) 423–429

[38] A. Garcia-Maraver, D. Salvachúa, M.J. Martínez, L.F. Diaz, M. Zamorano, Analysis of the relation between the cellulose, hemicellulose and lignin content and the thermal behavior of residual biomass from olive trees, Waste Management 33 (2013) 2245–2249